Mechanics of Advanced Materials and Structures

ISSN: (Print) (Online) Journal homepage: https://www.tandfonline.com/loi/umcm20

A high-precision apparatus for dimensional characterization of highly stable materials in space applications

Baolong Sun, Hansi Zhang, Chuang Xue & Weihui Shang

MECHANICS OF ADVANCED MATERIALS AND STRUCTURES
2022, VOL. 29, NO. 25, 4299–4309
https://doi.org/10.1080/15376494.2021.1926605

Taylor & Francis
Taylor & Francis Group

Check for updates

ORIGINAL ARTICLE

A high-precision apparatus for dimensional characterization of highly stable materials in space applications

Baolong Sun[a], Hansi Zhang[b], Chuang Xue[a], and Weihui Shang[c]

[a]Changchun Institute of Optics, Fine Mechanics and Physics, Chinese Academy of Sciences, Changchun, China; [b]Electromechanical Technology Institute, Jilin Agricultural Machinery Research Institute, Changchun, China; [c]Changchun Long Aerospace Composite Materials Co., Ltd., Changchun, China

ABSTRACT

We present an apparatus for high-accuracy and high-resolution absolute measurement of the linear coefficient of thermal expansion (CTE). Based on a displacement measuring interferometer (DMI) system, dimensional changes of a tubular shaped specimen under controlled thermal conditions can be characterized. Our measurement apparatus was located in a vacuum where the test specimen could be controlled in a temperature range from 20 to 40 °C. We measured the CTE of a quartz tube by using the DMI system with a temperature variation close to 4 °C. The test result was $(3.888 \pm 0.1292) \times 10^{-7}$/°C with 99% confidence probability. The measured value of 3.89×10^{-7}/°C of the specimen taken from the above-mentioned quartz tube (DIL402 Expedis, NETZSCH) was within the confidence interval, which indicates that our apparatus not only has excellent repeatability but also has the correct absolute CTE value. The measurement uncertainty reached the 1.3×10^{-8}/°C level. Finally, a CTE test of carbon-fiber reinforced plastic (CFRP) tubes was conducted. The test result was $(1.218 \pm 0.0822) \times 10^{-7}$/°C with 99% confidence probability. The results show that we can manufacture CFRP tubes with a CTE of 0.12×10^{-6}/°C, which could be used for aeronautical and space structures.

ARTICLE HISTORY
Received 24 July 2020
Accepted 3 May 2021

KEYWORDS
CFRP; coefficient of thermal expansion; dimensional characterization; heterodyne interferometer; space structure

1. Introduction

The demand for lightweight design continues to increase in aeronautical and space structures, where the components are made up of composites instead of metals. Advanced carbon-fiber reinforced plastic (CFRP) materials are well suited for stable space structures due to their light weight, high stiffness and low coefficient of thermal expansion (CTE). In space telescope structures, all optical components and scientific instruments are installed on a truss structure. The deformation of each component directly affects the relative position between the primary mirror and secondary mirror. Therefore, it is very important to ensure the stability of the telescope truss structure to obtain the desired quality of the optical images.

In the case of our telescope structure, the secondary mirror is supported at the required five meters vertex separation from the primary mirror by a lightweight truss structure. To make high-resolution observations of objects, the truss structure must be stable to a few micrometers. This implies an extremely low coefficient of thermal expansion, where the in-operation telescope temperature variation does not exceed 4 °C based on our level of thermal control. The configuration of the truss structure consists of frames, support tubes, and joints. Therefore, the allowable CTE of the support tube is approximately 0.1 ppm/°C. The support tubes had an 80 mm maximum outer diameter and a maximum length of 2000 mm.

Generally, the CTE of materials can be assumed to be approximately constant for a relatively small range of temperature variations. In this case, the CTE of the material in a small range of temperature variations (called the average CTE) is expressed in terms of linear deformation. Optical interference measurements provide great improvement in resolution and precision compared to those relying on optical imaging [1–3] and speckle pattern interferometry [4, 5]. Based on wavelength measurements, optical interferometers [6–9] have been used to obtain accurate deformations of structures through noncontact measurement. By controlling the geometrical error sources and environmental fluctuations, the accuracy of optical interferometers can reach a few nanometers. Badami and Linder [10] discussed significant error sources and made highly accurate absolute measurements of CTE. Schödel [11] reviewed a thermal expansion measurement system consisting of precision interferometer. Cordero et al. [12], Schuldt et al. [13], Spannagel et al. [14], and Zhang et al. [15–17] developed high-precision displacement measurement systems based on the heterodyne interferometer, which provide high accuracy and are easy to implement.

In the existing laser interferometry technology, the reflector mirrors and the interferometer component are

CONTACT Baolong Sun sunbaolong2015@163.com Changchun Institute of Optics, Fine Mechanics and Physics, Chinese Academy of Sciences, Dong-Nanhu Road 3888, Changchun, China, 130033

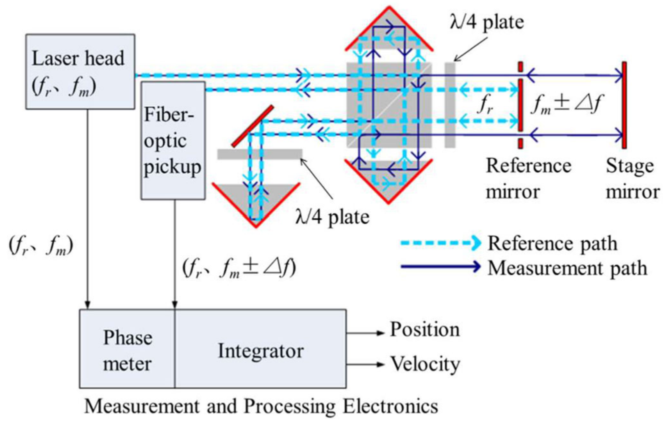

Figure 1. Working principle of the DMI.

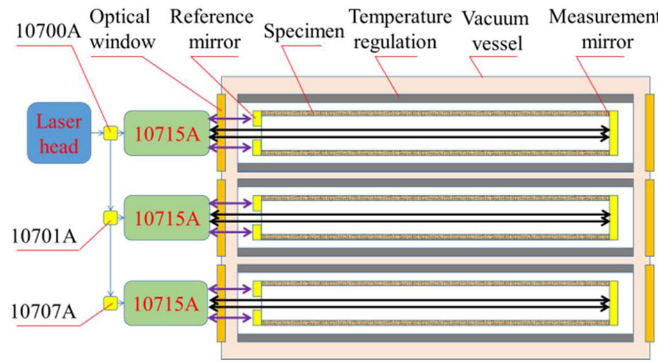

Figure 2. Schematic of the DMI system installation.

located in the same environment, in a vacuum environment or in a laboratory atmosphere environment. In this article, the reflector mirrors (measurement mirror and the reference mirror) are located in a vacuum system, and the interferometer component is located outside the vacuum system, that is, in the laboratory atmosphere environment, which not only meets the high-precision measurement requirements of the measurement path (from the measuring mirror to the reference mirror) in a vacuum environment but also makes the interferometer component work under a stable normal temperature and pressure. This avoids the influence of high vacuum and temperature changes in the test environment on the stability of the interferometer to improve the measurement accuracy. In addition, we improved the design of the reflector mirror installation method at both ends of the sample in a prior article. The method leads to high thermal stability and reduces the influence of temperature changes on the deflection of the reflector mirrors extremely well. At the same time, it can meet the measurement requirements of samples of various sizes and specifications, which improves the versatility and practicability of the measurement apparatus. The apparatus used a laser interferometer to measure length variation and a Pt100 temperature sensor to record temperature variation. To date, the apparatus has been used to characterize tubes of CFRP.

2. Measurement method

The displacement measuring interferometer (DMI) system of our apparatus consists of highly stable interferometers, reflector mirrors, fiber-optic pickups, a dual-mode laser head, and supporting electronics. The interferometer is based on a highly symmetric design, which was implemented to achieve differential length variation measurements between the reference and measurement arms. The differential interferometer allowed differential measurements to be made between two plane mirrors (the reference plane mirror and the measurement plane mirror). The major benefit of the differential interferometer was that the optical path was common to both the reference and the measurement beams (as shown in Figure 1). This enabled the interferometer to be extremely tolerant to changes such as thermal expansion or changes in air characteristics. Since the measurement of the beam traveled twice between the interferometer and the plane mirror, the resolution of the measurement was twice that of a linear or single-beam interferometer. In this article, the measuring mirror and the reference mirror are both located outside the interferometer. Through the relative movement between the measuring mirror and the reference mirror at both ends of the sample, accurate measurement of the deformation of the sample is realized. The measuring mirror and the reference mirror are located in the vacuum system. The interferometer is located outside the vacuum system (in a laboratory atmosphere environment), which not only ensures that the measurement path (from the measuring mirror to the reference mirror) is in a vacuum environment, but also realizes that the interferometer works under a stable normal temperature and pressure, which solves the contradiction that the measurement path requires a vacuum environment and the interferometer needs to work under a stable normal temperature and pressure.

In this study, a dual-mode laser head was used to produce a laser beam, which consists of two orthogonally polarized components [18]; the reference frequency, identified as f_r, is orthogonally polarized to the measurement frequency f_m. f_r traveled along the reference path, while f_m traveled along the measurement path (as shown in Figure 1).

Our apparatus was designed to accurately measure the CTE of the specimen. Figure 2 shows the schematic of the present thermal deformation measurement system. The specimen was maintained inside a vacuum vessel with a temperature control unit to simulate the space environment. An optical window was installed on the vacuum vessel for the laser light to pass through.

To improve the efficiency of the measurement, our apparatus simultaneously measures three specimens. The DMI system consists of a laser head, three differential interferometers, two beam splitters, a beam bender, three receivers, a PCI laser board, and a specimen with a reference mirror and measurement mirror clamped at both ends. The specimen was placed inside a heating cover with a resistance heater for temperature control. The temperature test function was applied to the heating system, and the temperature variation (defined as ΔT) of the specimen was measured by a Pt100 temperature sensor. Two mirrors were clamped at the ends of the specimen at an original distance L_0; its length variation, ΔL, when exposed to temperature changes

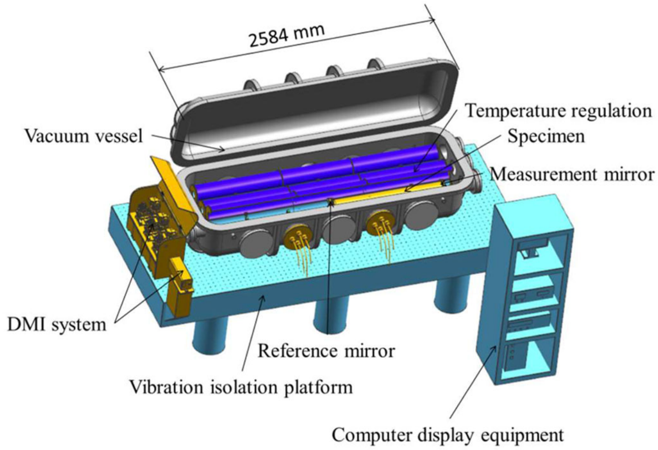

Figure 3. Schematic of the hardware platform layout.

was measured by the DMI system. The most general definition of CTE is given in the ASTM standard [19,20]:

$$\alpha_{T_0,T} = \frac{(L_T - L_{T_0})}{L_0(T - T_0)} = \frac{\Delta L}{L_0 \Delta T} \quad (1)$$

where $\alpha_{To,T}$ is the average CTE over the temperature range from T_0 to T.

3. Experimental set-up

The whole apparatus was placed in a clean room with constant temperature and humidity. The hardware platform consists of three subsystems, namely, the measurement subsystem, the structure subsystem, and the environment subsystem. Each subsystem included two units that perform specific functions. A schematic diagram of the hardware platform layout is shown in Figure 3.

The specimen and the heating subsystem were located inside the vacuum vessel. A heat tunnel that surrounded the specimen was oxidized to black to easily transfer heat through radiation.

3.1. Measurement subsystem

The measurement subsystem included the length variation measurement unit and the temperature measurement unit.

3.1.1. Length variation measurement unit

The DMI system consisted of a laser head (Agilent 5517DL), three interferometers (Agilent 10715A differential interferometer), two beam splitters (Agilent 10700A 33% beam splitter and Agilent 10701A 50% beam splitter), a beam bender (Agilent 10707A), three receivers (Agilent E1709A remote high-performance receiver), a PCI laser board (Agilent N1230A), a reference mirror and a measurement mirror clamped at the ends of the specimen. Our apparatus was designed for measuring the CTE of cylindrical tubes with a maximum outer diameter of 100 mm, minimum internal diameter of 30 mm, and maximum length of 2200 mm.

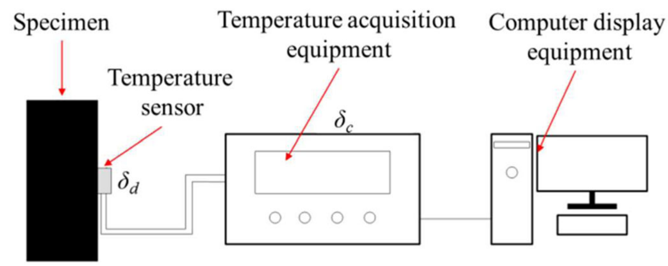

Figure 4. Schematic of the temperature measurement unit.

Because Zerodur has a very small CTE ($<0.1 \times 10^{-6}$/°C), it was selected as the material for the measuring mirror and the reference mirror. Zerodur can be polished and coated directly on the reflective surface. Invar was selected as the material for the support structure of the DMI system. It has a very small CTE ($<0.1 \times 10^{-6}$/°C).

3.1.2. Temperature measurement unit

The temperature measurement unit consisted of temperature sensors, temperature acquisition equipment, and computer display equipment (as shown in Figure 4). The error of the whole temperature measurement unit consisted of the measurement error of the temperature sensor and the error of the temperature acquisition equipment.

The temperature measurement error δ_T can be calculated by the following formula:

$$\delta_T = \sqrt{\delta_d^2 + \delta_c^2} \quad (2)$$

where δ_d represents the measurement error of the temperature sensor, and δ_c represents the error of the temperature acquisition equipment.

The platinum resistance Pt100 was selected as the temperature sensor in the temperature measuring system. Because the highest precision of class B platinum resistance Pt100 is 0.3 °C, it was necessary to select the platinum resistance to meet the requirements of high-precision measurement through a calibration test. The calibration results of platinum resistance and its error are shown in Figure 5.

The precision of platinum resistance Pt100 reached 0.02 °C through the calibration test. Therefore, $\delta_d = 0.02$ °C.

The EX1266A high-density switching measuring system was selected as the main temperature collecting box. The EX1200-3048 and EX1200-3072 multichannel converters were selected as the temperature collecting modules. The measurement temperature range of the specimen was from 20 to 40 °C, and its measurement error was ±0.10 °C in this temperature range. Therefore, $\delta_c = 0.10$ °C.

The error of the whole temperature measuring system was approximately 0.102 °C.Two insulated adhesive tapes were used in the temperature measuring unit. To avoid contact resistance, one insulated adhesive tape was glued between the platinum resistance and tested surface, and another insulated adhesive tape was used to fix the platinum resistance on the surface of the specimen.

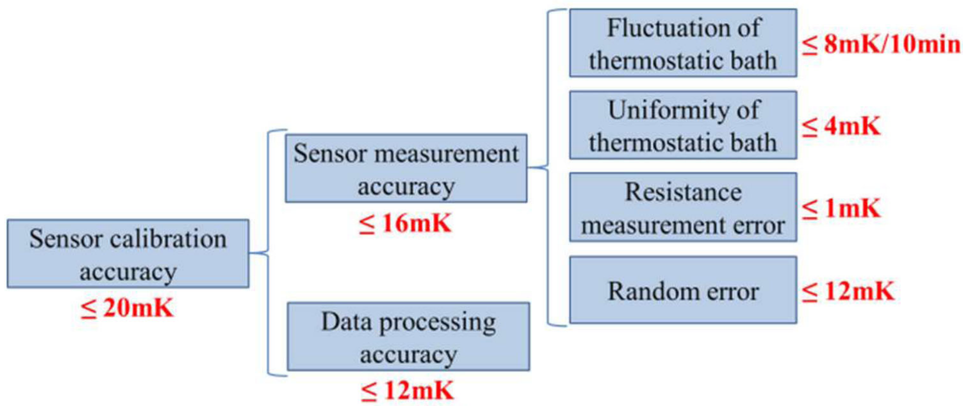

Figure 5. Schematic of sensor accuracy calibration.

3.2. Environment subsystem

The environment subsystem consisted of the temperature regulation unit and the vacuum vessel unit. The temperature regulation unit was maintained inside the vacuum vessel unit where the heat was only transferred *via* radiation.

3.2.1. Temperature regulation unit

The temperature regulation unit consisted of a heating cover, a resistance heater, a temperature control sensor, multilayer thermal insulation components, and a power supply. The heating cover used the resistance heater to heat the inside surface, and the inside surface was oxidized to black to improve the uniformity of the radiation of the energy. The heating cover had a heating ability of 40 °C, and the heating cover was provided with multiple heating zones (as shown in Figure 6).

The temperature control sensor and the resistance heater were pasted on the outer surface of the heating cover. The outer surface of the heating cover was wrapped with five layers of multilayer heat insulation components. The temperature measurement and control equipment were placed outside the vacuum vessel, and a cable transmission signal was used between the equipment inside and outside the vessel.

3.2.2. Vacuum vessel unit

The main body of the vacuum vessel was a rectangular box of dimensions 2584 mm × 754 mm × 676 mm (as shown in Figure 7). The box was made up of two parts. The upper part of the box was a rectangular cover plate that could be hoisted. The lower part of the box was connected with the bottom vibration isolation platform. The vacuum vessel was operated through a molecular pump at pressures below 10^{-2} Pa to avoid air turbulence, and the refractive index was nearly unity.

Three optical windows were placed on each side of the vacuum vessel unit for the laser light to pass through (as shown in Figure 8). The window glass was HPFS7980 (Corning), the diameter was 150 mm and thickness was 30 mm.

3.3. Structure subsystem

The structure subsystem included two units, the vibration isolation unit and the supporting unit. The function of the vibration isolation unit was to reduce the influence of vibration. The supporting unit provided stable support for the test units. Furthermore, the supporting unit also reduced the deformation caused by gravity.

3.3.1. Vibration isolation unit

The vibration isolation platform adopted the ZDT-P-36-14 optical platform (as shown in Figure 9). Its size was 3600 mm × 1400 mm × 800 mm. The natural frequency of the vibration isolation platform was 1 Hz.

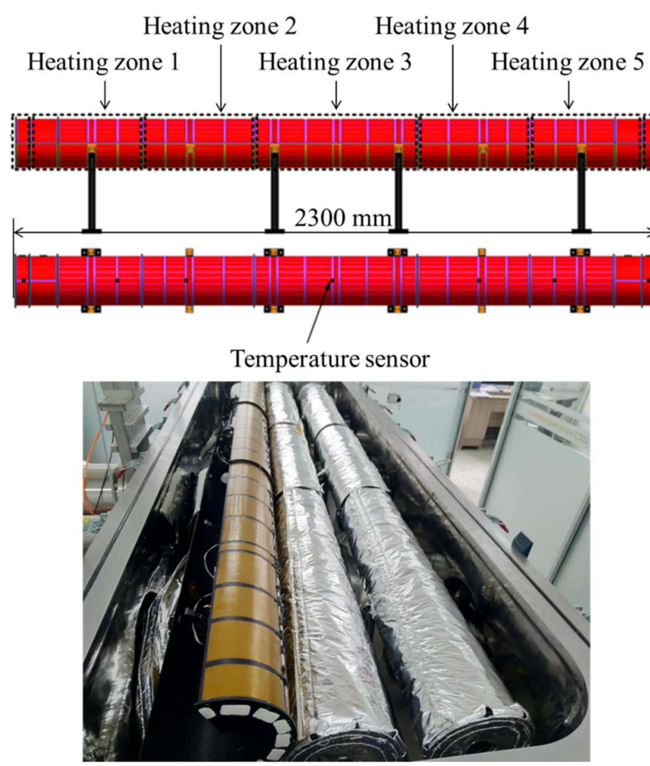

Figure 6. Schematic of the temperature regulation unit.

Figure 7. Front view of the vacuum vessel unit.

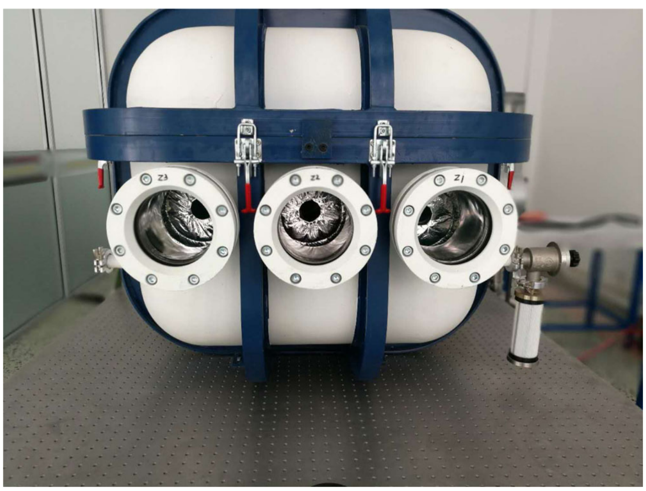

Figure 8. Side view of the vacuum vessel unit.

Figure 9. Vibration isolation platform.

3.3.2. Supporting unit

The supporting unit mainly consisted of a mirror support structure, specimen support structure, and DMI system support structure.

The two ends of the specimen were the measuring mirror and the reference mirror, which meant that the reflector mirrors were assembled directly to the end of the specimen. The mirror support structure is shown in Figure 10 and consisted of fastening screws, pins, adjusting screws, mirror adjusting seats, briquettings, mirror seats, and springs.

The specimen support structure used a structure with low thermal conductivity of titanium alloy and polyimide, which is shown in Figure 11. Polyimide thermal insulation pads were selected to increase the contact thermal resistance, the thermal resistance of the supporting structure was increased by reducing the cross-sectional area of the titanium alloy, and the final thermal resistance reached 120 °C/W.

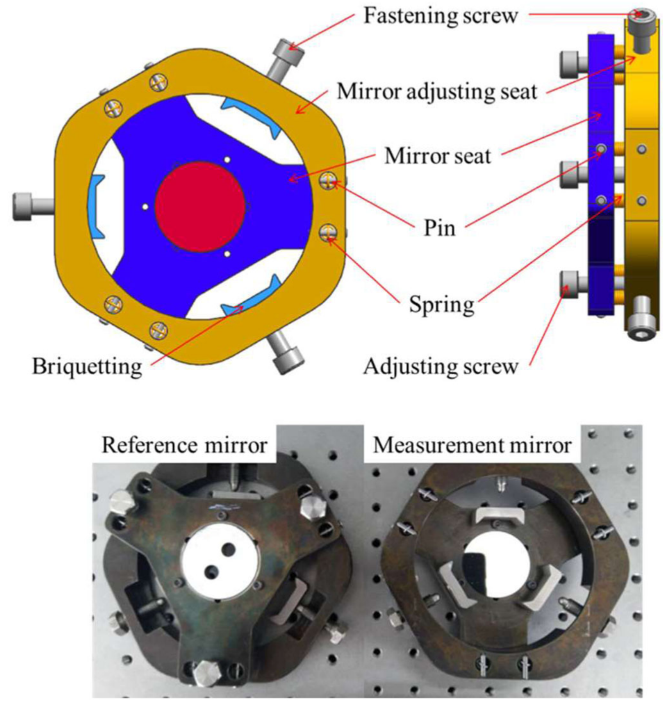

Figure 10. Support structure of the mirror.

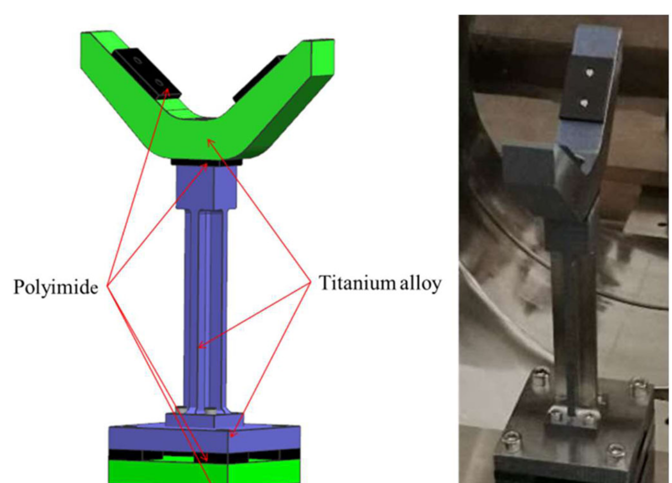

Figure 11. Support structure of the specimen.

The supporting structure of the DMI system mainly refers to the supporting structure of the interferometer, the beam splitter, the beam bender, and the laser. The support structures of the interferometer, beam splitter, and beam bender were fixed structures, as shown in Figure 12.

3.4. Uncertainty evaluation of the system

The measurement uncertainty can be estimated by combining the uncertainty of the measurement of the temperature

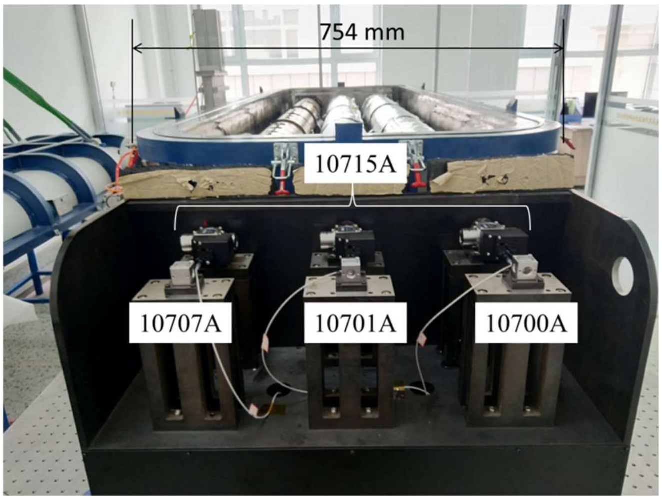

Figure 12. Support structure of the DMI system.

variation, initial length, and length variation. Then, the combined uncertainty can be determined by taking the square root of the standard deviation of the sum of the square of each term. Therefore, the measurement uncertainty of the CTE using the DMI system was estimated with the following formula:

$$u_\alpha = \sqrt{\left(\frac{1}{L_0\Delta T}\right)^2 u_{\Delta L}^2 + \left(\frac{\Delta L}{L_0(\Delta T)^2}\right)^2 u_{\Delta T}^2 + \left(\frac{\Delta L}{L_0^2\Delta T}\right)^2 u_{L_0}^2} \tag{3}$$

The apparatus errors of DMI systems originated from the components, including the laser head, data acquisition boards, and interferometer optics. This type of uncertainty was usually provided by the component's manufacturer [18]. If the length of the laser beam path and the deflection of the light spot were considered, it was estimated that the cosine error due to the worst case of mirror tilt was not more than 1.5 nm. A series of zero-drift measurements were performed under vacuum conditions with a long-term stability of approximately 6 nm.

When ΔT was 4 °C with $u_{\Delta T}$ of 0.102 °C, L_0 was 0.564 m with u_{L0} of 0.1 mm and α was approximately 0.4×10^{-6}/°C (quartz tube used for subsequent uncertainty verification). In this case, the measurement uncertainty of the DMI system was estimated and is listed in Table 1. Table 1 shows that the measurement uncertainty of CTE was approximately 1.18×10^{-8}/°C.

4. Measurements and results

To characterize our measurement apparatus, quartz and CFRP were used as highly stable materials to verify the measurement uncertainty of our apparatus. According to the measured CTE results of CFRP, the theoretical calculation model of CFRP was revised.

4.1. Measurements of quartz

A sample tube made of quartz was used as a highly stable material to verify the measurement uncertainty. We also used the DIL402 Expedis (NETZSCH) to measure the CTE of a small specimen, which was taken from the end of the above-mentioned quartz tube. The test results were compared with those of our apparatus. A schematic of the comparative test diagram is shown in Figure 13.

4.1.1. Specimen preparation

The quartz tube had an outer diameter of 60 mm, wall thickness of 5 mm, and length of 564 mm (as shown in Figure 14). The surface of the specimen was clean, ensuring that dust attached to the surface of the specimen was removed. Under the premise of confirming that the surface of the sample was not contaminated by other substances, we installed the measurement mirror and the reference mirror to the end of the specimen.

The CTE of the specimen taken from the end of the quartz tube was measured by using DIL402 Expedis (NETZSCH). The length of the sample was 21 mm, and the cross-section envelope was less than 6 mm in diameter. The test result of DIL402 Expedis (NETZSCH) showed that the average CTE of the specimen was approximately 0.389×10^{-6}/°C (as shown in Figure 15).

4.1.2. Results for the quartz specimen

Six independent repeated tests were carried out with a quartz tube at room temperature (approximately 20 °C), and then the uncertainty evaluation of our apparatus was accomplished according to the Type-A evaluation of measurement uncertainty. For the CTE measurements, the temperature variation was close to 4 °C from room temperature, and the specific temperature variation value was limited by the temperature regulation unit. Figure 16 shows the test curves of six independent repeated CTE tests.

The six measurements of the quartz tube were 0.3965×10^{-6}/°C, 0.3818×10^{-6}/°C, 0.3841×10^{-6}/°C, 0.3794×10^{-6}/°C, 0.3956×10^{-6}/°C, and 0.3954×10^{-6}/°C. The error was the result of the assembly process and conservative assumptions about system impact (such as nonuniform temperature of the sample tube and nonlinearity of the interferometer). The average value of the test results was 0.3888×10^{-6}/°C (as shown in Table 2). The experimental standard deviation can be calculated by the following formula:

$$\sigma_{\bar{\alpha}} = \sqrt{\frac{\sum_{i=1}^{n}(\alpha_i - \bar{\alpha})^2}{n(n-1)}} \tag{4}$$

where $n = 6$, and other calculation results can be obtained from Table 2.

The standard uncertainty of $\bar{\alpha}$ was 3.207×10^{-9}/°C. The expanded uncertainty of our apparatus can be calculated by the following formula [21]:

$$U_p = k_p\sigma_{\bar{\alpha}} = t_p(\nu)\sigma_{\bar{\alpha}} \tag{5}$$

Table 1. Uncertainty estimation of the CTE measurement using the DMI system.

Measurands	Uncertainty		Contribution
DMI uncertainty ($u_{\Delta L}$)	Long-term wavelength stability	11.3 nm	
	Electronics error	0.15 nm	
	Optics nonlinearity	2.2 nm	
	Thermal drift error	2 nm	5.85×10^{-9}/°C
	Cosine error	1.5 nm	
	Long-term error	6 nm	
	Total	13.2 nm	
Temperature uncertainty ($u_{\Delta T}$)	0.102 °C		1.02×10^{-8}/°C
Length uncertainty (u_{L0})	0.1 mm		7.09×10^{-11}/°C
	Combined standard uncertainty (u_α)		1.18×10^{-8}/°C

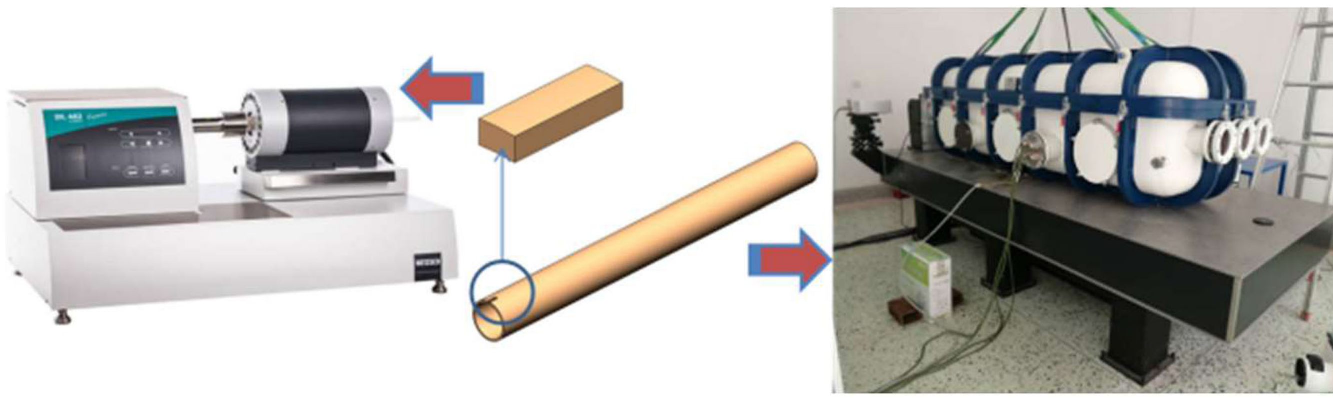

Figure 13. Schematic of the comparative test.

Figure 14. Tube of quartz.

where k_p is the coverage factor when the coverage probability is p, and p is 0.99 in this paper. ν is effective degree of freedom, and ν is 5 in this paper. The $t_{0.99}(5)$ is 4.03 from a t-distribution table.

The expanded uncertainty $U_{0.99}$ was 1.2924×10^{-8}/°C. Therefore, the measurement result of the quartz tube can be expressed as $(3.888 \pm 0.1292) \times 10^{-7}$/°C with 99% confidence probability. That is, the 99% confidence interval was from 3.7588×10^{-7}/°C to 4.0172×10^{-7}/°C. The measured value of 0.389×10^{-6}/°C of DIL402 Expedis (NETZSCH) is within that interval, which indicates that the CTE measurements of our apparatus not only had excellent repeatability but also had the correct absolute CTE value.

4.2. Measurements of CFRP

We measured the CTE of a CFRP tube, which was specifically designed to fulfill our space telescope thermal stability

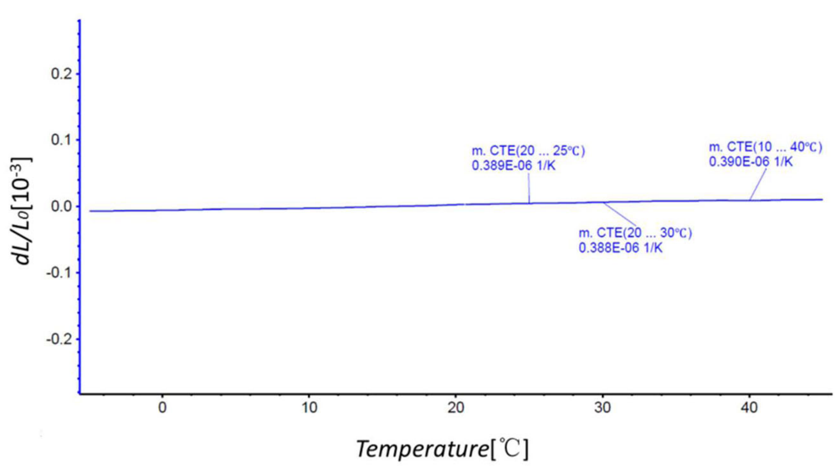

Figure 15. Test result of DIL402 Expedis for quartz specimen.

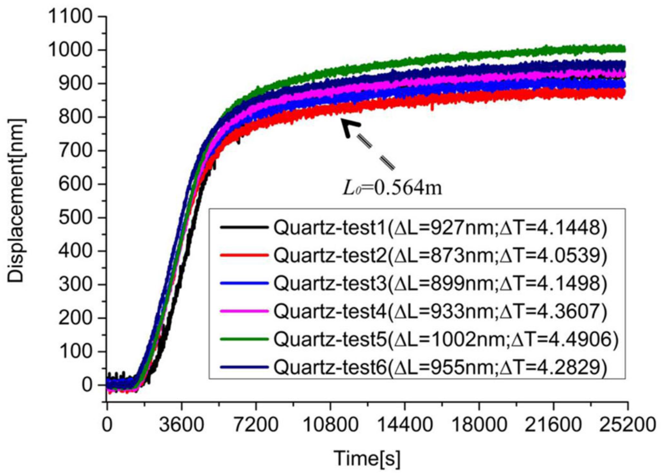

Figure 16. Displacement variation versus time curves of six independent repeated tests of quartz tube.

Table 2. Results of six independent repeated tests on quartz tube.

No.	α_i	$v_i = \alpha_i - \bar{\alpha}$
1	3.965×10^{-7}/°C	7.7×10^{-9}/°C
2	3.818×10^{-7}/°C	-7.0×10^{-9}/°C
3	3.841×10^{-7}/°C	-4.7×10^{-9}/°C
4	3.794×10^{-7}/°C	-9.4×10^{-9}/°C
5	3.956×10^{-7}/°C	6.8×10^{-9}/°C
6	3.954×10^{-7}/°C	6.6×10^{-9}/°C
Average ($\bar{\alpha}$)	3.888×10^{-7}/°C	

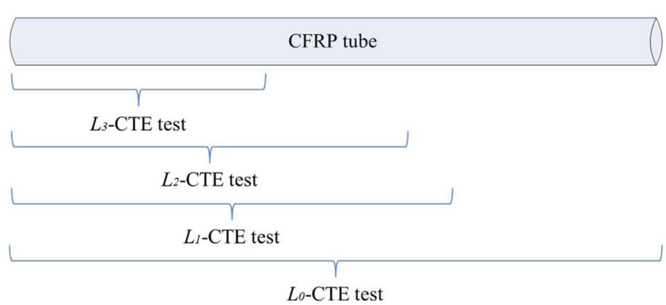

Figure 17. Schematic of comparative test diagram.

requirement with an ultralow expansion coefficient. By cutting the produced CFRP tube into different lengths, we measured the CTE of CFRP at different lengths. The measurement uncertainty of our apparatus was evaluated by the consistency of the measurement results. A schematic of the comparative test diagram is shown in Figure 17.

4.2.1. Specimen preparation

The lamination angles of the CFRP tube were $(0°/+61°/0°/0°/-61°/0°)_{4s}$, where the ±61° layers were made up of T700SC prepreg, and the 0° layers were made up of M40JB prepreg. The resin matrix was medium-temperature curing cyanate ester resin, and the curing temperature was 130 °C. The theoretical CTE of the tube was 0.113×10^{-6}/°C, the length of the tube was 2169 mm, the outer diameter was 80 mm, and the wall thickness was 4.8 mm (as shown in Figure 18). Due to the high requirements for quantitative control of the tubes in this program, the use of hot-melt prepreg for laying and forming achieved stable control of thickness and fiber volume content. In addition, the hand layup M40JB plies and the machine-applied pre-impregnated T700SC plies were selected as the molding process for composite tubes to control the stability of the axial thermal expansion coefficient.

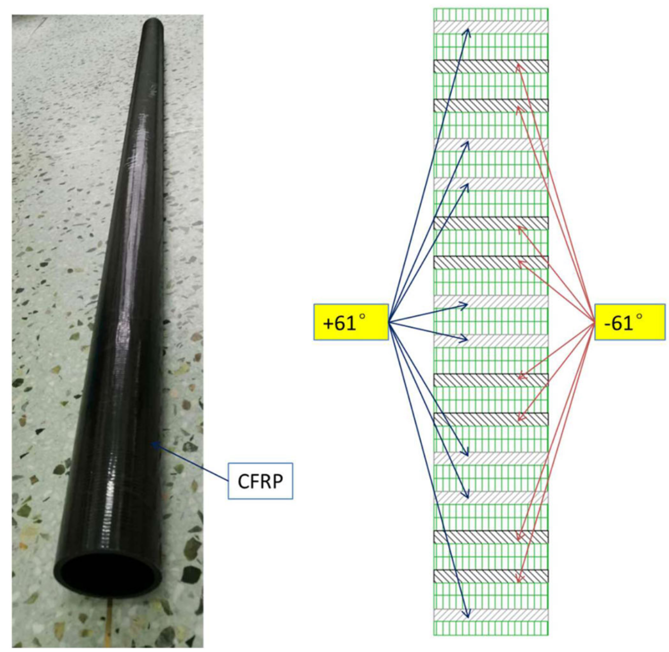

Figure 18. The tube of CFRP.

We conducted multiple sets of measurements on the CFRP tube. The specific experimental plan is shown in Figure 19.

The produced 2169 mm CFRP tube was gradually cut short to 1560 mm, 1523 mm, and 963 mm. Among them, 2169 mm, 1560 mm, and 963 mm were used to measure the consistency at different lengths. Six independent repeated tests were carried out under a length of 1523 mm, and then the uncertainty evaluation of our apparatus was accomplished according to the Type-A evaluation of measurement uncertainty.

4.2.2. Results for CFRP specimen

To certify the consistency of CTE at different lengths, three CTE tests of 2169 mm, 1560 mm, and 963 mm were conducted at room temperature (approximately 20 °C). For CTE measurements, the temperature variation was close to 4 °C. Figure 20 shows the test curves of the CFRP tube at different lengths.

The measured CTEs of the CFRP tubes were 0.1161×10^{-6}/°C (2169 mm), 0.1289×10^{-6}/°C (1560 mm), and 0.1288×10^{-6}/°C (963 mm), which indicates that the CTE measurement of our apparatus had excellent repeatability.

Six independent repeated tests were carried out with the CFRP tube at room temperature (approximately 20 °C) at a length of 1523 mm, and the temperature variation was close to 4 °C from room temperature. Figure 21 shows the test curves of six independent repeated CTE tests.

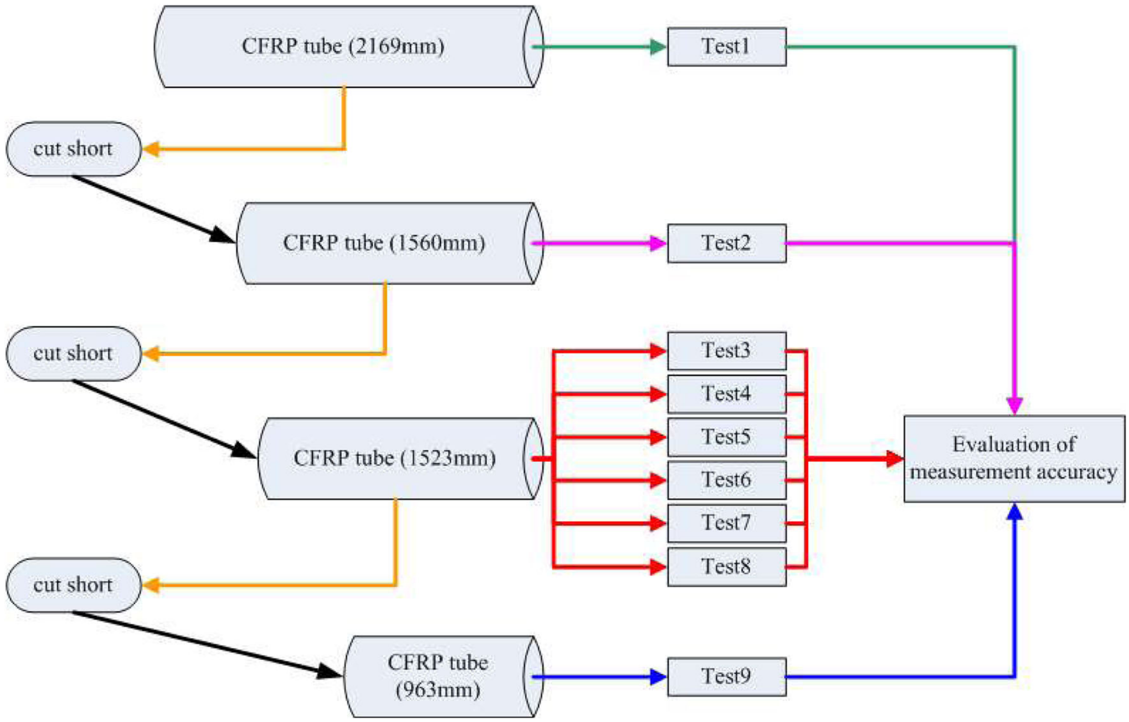

Figure 19. Schematic diagram of the specific experimental plan.

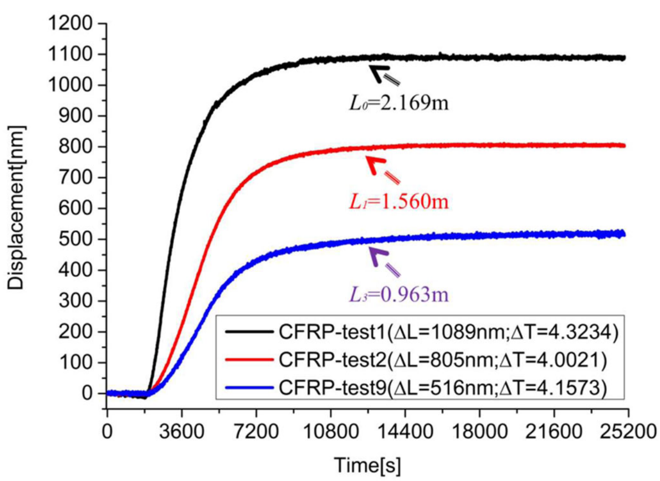

Figure 20. Displacement and temperature variation versus time curve of the CFRP tube at different lengths.

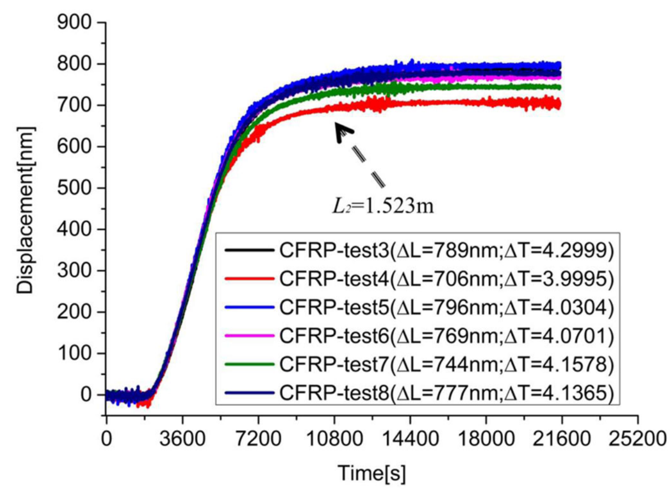

Figure 21. Displacement variation versus time curves of six independent repeated tests of the CFRP tube.

The six measurements of the CFRP tube were $0.1205 \times 10^{-6}/°C$, $0.1159 \times 10^{-6}/°C$, $0.1297 \times 10^{-6}/°C$, $0.1241 \times 10^{-6}/°C$, $0.1175 \times 10^{-6}/°C$, and $0.1233 \times 10^{-6}/°C$. The average value of the test results was $0.1218 \times 10^{-6}/°C$ (as shown in Table 3). The experimental standard deviation can be calculated by formula (4).

The standard uncertainty of $\bar{\alpha}$ was $2.041 \times 10^{-9}/°C$. The expanded uncertainty of our apparatus can be calculated by formula (5). The expanded uncertainty $U_{0.99}$ was $0.8224 \times 10^{-8}/°C$. Therefore, the measurement result of the CFRP tube can be expressed as $(1.218 \pm 0.0822) \times 10^{-7}/°C$ with 99% confidence probability. That is, the 99% confidence interval was from $1.1361 \times 10^{-7}/°C$ to $1.3001 \times 10^{-7}/°C$. The measured values of the CFRP tube at different lengths were within this interval, which indicates that the CTE measurement of our apparatus had excellent repeatability.

Table 3. Results of six independent repeated tests of the CFRP tube.

No.	α_i	$v_i = \alpha_i - \bar{\alpha}$
1	$1.205 \times 10^{-7}/°C$	$-1.3 \times 10^{-9}/°C$
2	$1.159 \times 10^{-7}/°C$	$-5.9 \times 10^{-9}/°C$
3	$1.297 \times 10^{-7}/°C$	$7.9 \times 10^{-9}/°C$
4	$1.241 \times 10^{-7}/°C$	$2.3 \times 10^{-9}/°C$
5	$1.175 \times 10^{-7}/°C$	$-4.3 \times 10^{-9}/°C$
6	$1.233 \times 10^{-7}/°C$	$1.5 \times 10^{-9}/°C$
Average ($\bar{\alpha}$)	$1.218 \times 10^{-7}/°C$	

The theoretical CTE value of $0.113 \times 10^{-6}/°C$ is not within the 99% confidence interval of the measurement results, but it was very close. Our measurement results can be interpreted as limitations in the manufacturing process of the CFRP tube. Because the plies were alternately laid on top of each other during the manufacturing process, the CFRP was inhomogeneous and anisotropic. The manufacturing process included several errors contributing to the obtained CTE values, such as the fiber resin percentage and the angle of the fiber layer relative to the tube axis. This theoretical value was based on a well-established database for CFRP materials. Therefore, we subsequently revised the theoretical calculation model based on the measurement results.

5. Conclusion

The measurement apparatus prepared in this study was designed to measure the thermal expansion of specimens in a simulated space environment using a DMI system. The experimental results demonstrated the effectiveness, practicability and measurement uncertainty of the experimental apparatus, which can reach the 10^{-8}/°C level. The design of the sample tube support and heating subsystem enabled accuracy to the nanometer level, which can be used to characterize the ultra-stable materials with a CTE greater than 10^{-8}/°C.

This paper solves the contradiction problem that the measurement path (from the measuring mirror to the reference mirror) requires a vacuum environment and the interferometer needs to work under a stable normal temperature and pressure. It not only meets the high-precision measurement requirements of the measurement path in a vacuum environment but also makes the interferometer work under a stable normal temperature and pressure. It avoids the influence of high vacuum and temperature changes in the test environment on the stability of the interferometer to improve the measurement accuracy, and improves the measurement accuracy of the order of 10^{-7}/°C in the existing technology to the order of 10^{-8}/°C. This article improves the design of the reflector mirror installation method at both ends of the sample in a prior article. The method leads to high thermal stability and reduces the influence of temperature changes on the deflection of the reflector mirrors extremely well. At the same time, it can also meet the measurement requirements of samples of various sizes and specifications, which improves the versatility and practicability of the measurement apparatus and is conducive to the industrialization of this technology. This kind of measurement apparatus has improved the test ability of approximately 200 mm sample in the existing technology to the order of 2000 mm. In addition, for the measurement of this equipment uncertainty characterization, this paper has carried out detailed and careful experimental analysis methods and can also provide a reference for the experimental verification of related technical research.

Further improvements of the study are also planned. Most of the uncertainty comes from systematic effects, which are characterized by the nonuniform temperature of the specimen, nonlinearity of the interferometer and assembly process. Improving the temperature control scheme, interferometer stability and assembly process can improve the performance of the apparatus. Within the plan to improve the accuracy of our apparatus, a new apparatus concept for sub-ppb metrology is being studied.

Comparing the results of the theoretical calculation and the actual measured results of the CFRP tube, the theoretical model is revised according to the actual measured results. The experimental results of this study can also be used as the basis parameter for performance analysis and prediction for finite element simulation of truss frames composed of ultralow expansion coefficient CFRP tubes.

Funding

This work is supported by the program 'Research on Preparation Technology of High Performance Carbon Fiber Composite Material' of Changchun Institute of Optics, Fine Mechanics and Physics, Chinese Academy of Science.

ORCID

Baolong Sun http://orcid.org/0000-0003-1261-191X

References

[1] X. Chen, N. Xu, L. Yang, and D. Xiang, High temperature displacement and strain measurement using a monochromatic light illuminated stereo digital image correlation system, Meas. Sci. Technol., vol. 23, no. 12, pp. 125603, 2012. DOI: 10.1088/0957-0233/23/12/125603.

[2] C. H. Hwang, S. H. Wang, and W. C. Wang, On the in-plane displacement measurement by 3D digital image correlation method, Adv. Opt. Methods Exp. Mech., vol. 3, pp. 19–26, 2018.

[3] T. I. Lee, M. S. Kim, and T. S. Kim, Contact-free thermal expansion measurement of very soft elastomers using digital image correlation, Polym. Test., vol. 51, pp. 181–189, 2016. DOI: 10.1016/j.polymertesting.2016.03.014.

[4] L. Bruno, G. Bianco, and M. A. Fazio, A multi-camera speckle interferometer for dynamic full-field 3d displacement measurement: validation and inflation testing of a human eye sclera, Opt. Lasers Eng.., vol. 107, pp. 91–101, 2018. DOI: 10.1016/j.optlaseng.2018.03.012.

[5] C. Dong, K. Li, Y. Jiang, D. Arola, and D. Zhang, Evaluation of thermal expansion coefficient of carbon fiber reinforced composites using electronic speckle interferometry, Opt. Express, vol. 26, no. 1, pp. 531, 2018. DOI: 10.1364/OE.26.000531.

[6] T. Schuldt et al., Sub-nanometer heterodyne interferometry and its application in dilatometry and industrial metrology, Int. J. Optomechatronics., vol. 3, no. 3, pp. 187–200, 2009.

[7] V. Martelli, G. Bianchini, E. Natale, D. Scarpellini, and G. Ventura, A novel interferometric dilatometer in the 4–300 k temperature range: thermal expansion coefficient of srm-731 borosilicate glass and stainless steel-304, Meas. Sci. Technol., vol. 24, no. 10, pp. 105203, 2013. DOI: 10.1088/0957-0233/24/10/105203.

[8] R. Scholl and B. W. Liby, Using a Michelson interferometer to measure coefficient of thermal expansion of copper, Physics Teach., vol. 47, no. 5, pp. 306–308, 2009. DOI: 10.1119/1.3116844.

[9] Y. Lou, L. Yan, B. Chen, and S. Zhang, Laser homodyne straightness interferometer with simultaneous measurement of six degrees of freedom motion errors for precision linear stage metrology, Opt. Express, vol. 25, no. 6, pp. 6805, 2017. DOI: 10.1364/OE.25.006805.

[10] V. G. Badami and M. Linder, Ultra-high accuracy measurement of the coefficient of thermal expansion for ultra-low expansion materials, Proc. SPIE, vol. 4688, pp. 469–480, 2002.

[11] R. Schödel, Ultra-high accuracy thermal expansion measurements with PTB's precision interferometer, Meas. Sci. Techn. vol. 19, pp. 084003, 2008. DOI: 10.1088/0957-0233/19/8/084003.

[12] J. Cordero et al., Interferometry based high-precision dilatometry for dimensional characterization of highly stable materials, Meas. Sci. Technol., vol. 20, pp. 095301, 2009. DOI: 10.1088/0957-0233/20/9/095301.

[13] T. Schuldt et al., Picometre and nanoradian heterodyne interferometry and its application in dilatometry and surface metrology, Meas. Sci. Technol., vol. 23, no. 5, pp. 054008, 2012.

[14] R. Spannagel, M. Gohlke, T. Schuldt, U. Johann, and C. Braxmaier, 2012. CTE measurement setup with 10 ppb/k sensitivity for characterizing lightweight and highly stable materials for space applications, Proceedings of SPIE - The International Society for Optical Engineering, 84500Q-84500Q-7. DOI: 10.1117/12.926061.

[15] E. Zhang, B. Chen, J. Sun, L. Yan, and S. Zhang, Laser heterodyne interferometric system with following interference units for large x–y–θ planar motion measurement, Opt. Express, vol. 25, no. 12, pp. 13684, 2017. DOI: 10.1364/OE.25.013684.

[16] E. Zhang, B. Chen, H. Zheng, L. Yan, and X. Teng, Laser heterodyne interferometer with rotational error compensation for precision displacement measurement, Opt. Express, vol. 26, no. 1, pp. 90, 2018. DOI: 10.1364/OE.26.000090.

[17] E. Zhang, B. Chen, H. Zheng, and X. Teng, Laser heterodyne interference signal processing method based on phase shift of reference signal, Opt. Express, vol. 26, no. 7, pp. 8656, 2018. DOI: 10.1364/OE.26.008656.

[18] Agilent Technologies, Agilent Laser and Optics User's Manual, Volume II, fifth, part number 05517-90086 ed., July 2007.

[19] ASTM E228-95, Standard Test Method for Linear Thermal Expansion of Sopid Materials With a Vitreous Silica Dilatometer.

[20] ASTM E289-99, Standard Test Method for Linear Thermal Expansion of Rigid Solids with Interferometry.

[21] JJF 1059.1-2012, Evaluation and Expression of Uncertainty in Measurement.